Anti-icing ionogel surfaces: inhibiting ice nucleation, growth and adhesion

Journal:	*ACS Materials Letters*
Manuscript ID	tz-2020-00094g.R1
Manuscript Type:	Letter
Date Submitted by the Author:	12-Apr-2020
Complete List of Authors:	Zhuo, Yizhi; Norwegian University of Science and Technology, Department of Structural Engineering Xiao, Senbo; Norges teknisk-naturvitenskapelige universitet, Department of Structural Engineering Håkonsen, Verner; Norges teknisk-naturvitenskapelige universitet He, Jianying; Norges teknisk-naturvitenskapelige universitet, Zhang, Zhiliang; Norges teknisk-naturvitenskapelige universitet,

Anti-icing ionogel surfaces: inhibiting ice nucleation, growth and adhesion

Yizhi Zhuo,† Senbo Xiao,† Verner Håkonsen, Jianying He* and Zhiliang Zhang*

NTNU Nanomechanical Lab, Department of Structural Engineering, Norwegian University of Science and Technology (NTNU), Trondheim 7491, Norway.

KEYWORDS: ionogel, icephobicity, ice growth, ice nucleation, interfacial liquid

ABSTRACT: Delaying ice and frost formation is one of the key strategies to mitigate the hazards induced by ice accretion. The current surfaces for delaying ice formation rely on restricting heterogeneous ice nucleation, which fails in practical applications as dust and impurity from environments serve as undesired nucleation sites and thus promote ice nucleation. Herein, ionogel surfaces are prepared to not only inhibit ice nucleation but also control ice growth. At -20 ºC, the prepared surface enables an unconventional inward ice growth from the water droplet-air interface, resulting in a spherical cap ice rather than a normal pointy cap ice. Both experiments and molecular simulations confirm that the prepared ionogel surface can efficiently generate an interfacial liquid layer thanks to the inward ice growth and presence of ionic liquid. Such non-frozen interfacial liquid layer is desired for lowering ice adhesion and preventing frost formation. Consequently, the ionogel surface exhibits exceptional anti-frost abilities under cold humid environment (-20 ºC, importing gas: 60% RH at 20 ºC).

Ice and frost formation on exposed surfaces, such as on airplanes, ship hulls, power lines and constructions, can cause catastrophic damage.[1-4] It is well accepted that ice formation contains two sequential steps, namely rate-limiting ice nucleation (IN) and fast ice growth and recrystallization (IGR).[5] Recently, various surfaces that can delay IN have been developed to suppress the formation of ice, targeting the initial and limiting step of icing.[6, 7] Generally, IN initiates at the interface between water and other solid/liquid (heterogeneous nucleation), where the free energy barrier of nucleation is lower than in the bulk (homogeneous nucleation).[7] Hence, many efforts have been made to prepare surfaces for restricting heterogeneous IN.[6, 8-10] For example, superhydrophobic surfaces have been rationally designed to inhibit the heterogeneous IN by greatly reducing the actual solid-liquid contact area.[8, 11] Slippery liquid-infused porous surfaces (SLIPS) also have been used to suppress the heterogeneous IN owing to the improved smoothness and reduced possible nucleation sites.[12] Unfortunately, such surfaces are inevitably exposed to the ubiquitous dust and impurity in practical applications, bringing undesired nucleation sites and thus promoting ice nucleation.[13-16] Moreover, even minor changes in environmental conditions, such as humidity and gas flow, can trigger IN.[17] Therefore, solely suppressing the heterogeneous IN is far from enough to effectively prevent icing in real environment. Controlling the other key ice formation step, IGR, should be taken into account to mitigate ice formation.[18-22] For example, altering the growth direction of ice, i.e. making the ice grow from the droplet free-surface toward the droplet-substrate interface, can facilitate freezing water droplets spontaneous self-dislodging from the surface.[23] However, the change of ice growth direction relies on specific environmental conditions, such as artificially low environmental pressure, large heat convection and high substrate temperature, rather than surface intrinsic functionality. To date, surfaces that can efficiently inhibit IGR is still missing.

Herein, ionogel surfaces are prepared for inhibiting IN and IGR simultaneously. The ionic liquid of ionogel can diffuse to contacted water droplets and depress the freezing temperature at the interface, thus enabling an unconventional inward ice growth from the droplet-air interface towards droplet-ionogel interface and then facilitating the detaching of formed ice at -20 ºC. As confirmed by both experiments and atomistic simulation, during the freezing process, the diffused ions can be rejected to the unfrozen liquid phase, thereby generating a nonfrozen interfacial liquid layer with high concentration of ions. Molecular dynamics (MD) simulations further reveal that larger ions of the ionic liquid are easier to be rejected to the unfrozen phase, while a portion of smaller ions are trapped by the formed ice, leading to an increasing electric field against ice growth. Owing to the anti-freezing effect of the ionic liquid, ionogel surfaces exhibit exceptional anti-frost abilities under humid environment (-20 ºC, importing gas: 60% RH at 20 ºC).

To prepared ionogel, crosslinked gelatin (CG) is incorporated with 1-butyl-3-methylimidazolium bromide (BMImBr), as shown by the experimental details given in the Supporting Information (SI) (Figure S1-S2). For comparison and demonstrating the unique anti-icing/anti-frost properties of the prepared ionogel surfaces, hydrophobic ionogel (BIG) aluminum foil (Al), glass, polymethyl methacrylate (PMMA), polydimethylsiloxane (PDMS), as well as pure crosslinked gelatin (CG) are fabricated for testing. BIG consists of hydrophobic ionic liquid (1-Ethyl-3-methylimidazolium bis(trifluoromethylsulfonyl)imide, EMImTFSI) and

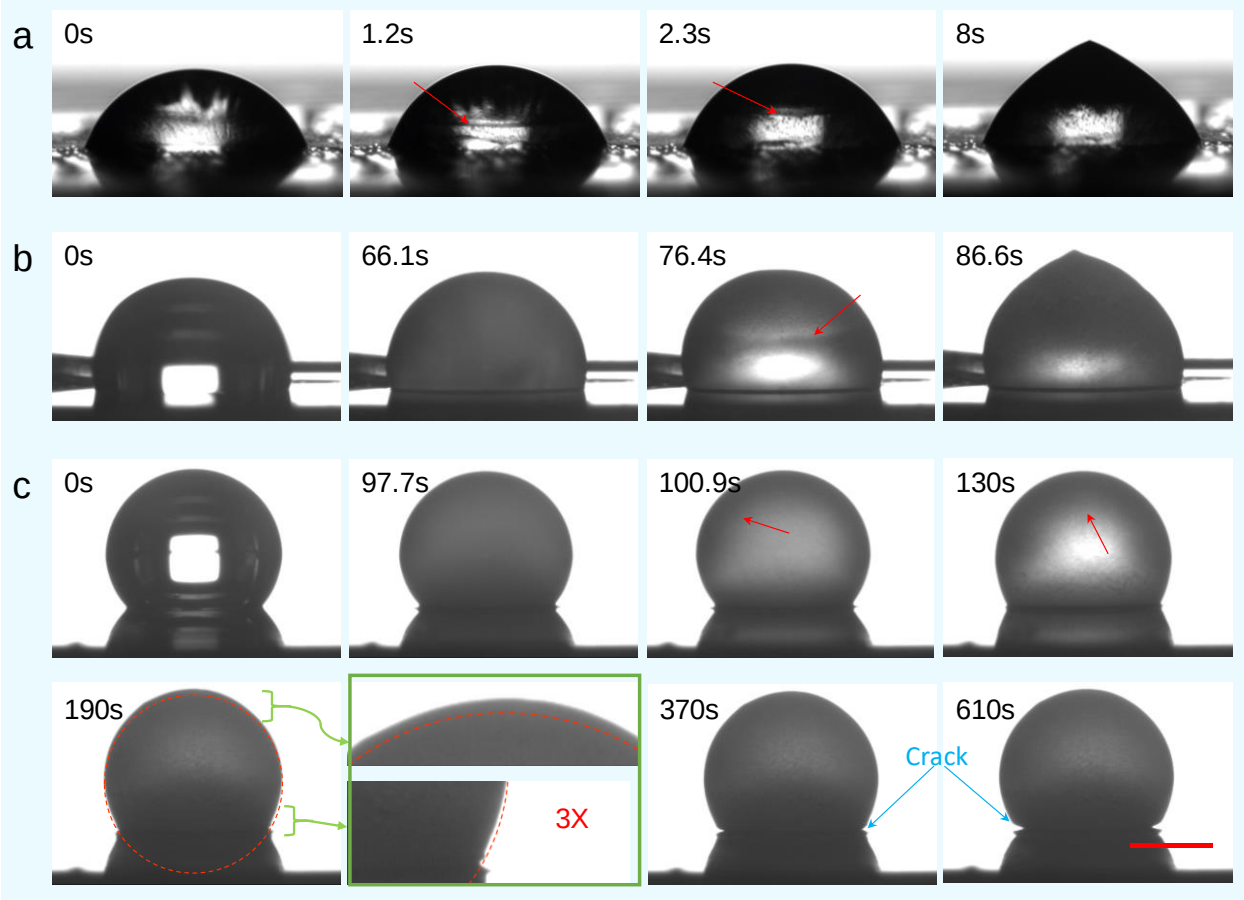

Figure 1. Ice nucleation and growth in single droplets on different cooled (-20 ºC) surfaces of Al (a), CG (b), and ionogel (c). The freezing front in each droplet is indicated by red arrows. Different parts of the droplet on the ionogel surface are enlarged and shown as insets (green frame) in (c). The red dashed curve in the panel of 190 s and the inset magnified images (green frame) is the shape outline of the droplet at 130 s. A crack (denoted by blue arrows in (c)) forms at the contact line due to the lifting of the droplet. All the figures share the same scale bar of 1 mm (red bar in the last panel of (c)), except the insets (green frame) which are enlarged 3 times. All the time in the upper-left corners of the images is real time of the example images.

hydrophobic polymeric matrix (Poly(vinylidene fluoride-co-hexafluoropropylene), PVDF-HFP) (Figure S1-S2).

Distinctive ice formation dynamics and a different ice pattern are observed on the ionogel surfaces, as indicated by the water droplets freezing processes shown in Figure 1 and Figure S3 & Movie S1-S5. As soon as the water droplets (same size; 3 μL) contact with the Al, glass, PMMA, PDMS and BIG surfaces at -20 ºC, IN occurs immediately followed by fast IGR. The fast ice formation on these surfaces can be attributed to the small pre-formed frost at -20 ºC (Movie S1-S5), which are large enough to serve as nucleation sites for fast ice growth, a commonly observed phenomenon in nature.[16] Importantly, ice growth starting from the solid-water interface on these surfaces results in a pointy top on all the frozen droplets (Figure 1a & 1b and Figure S3) due to the expansion of water upon upward freezing.[24] There is no sign of delay in IN or depression of IGR in any of these surfaces during the experiments. The CG surface interestingly shows a certain capability of delaying ice nucleation, as shown in Figure 1b, because hydrophilic CG can adsorb water molecules and restrict the mobility and rearrangement of them.[9, 25, 26] With the adsorption of water, hydrogen bonds are formed between water molecules and the CG polymer networks at the interface. The formation of ice nuclei from such bound water compared to free water requires additional energy, indicating the higher energetic barrier for nucleation. Consequently, the heterogeneous ice nucleation on CG surface is inhibited. Nucleation takes place after 66.1 s and the droplet suddenly becomes opaque within 0.1 s, as shown in Figure 1b and Movie S6. During this rapid process, a portion of liquid nucleates to form a slushy mixture of ice crystals and liquid, in which most of the generated latent heat is absorbed by the liquid and consequently rising its temperature synchronously.[17, 24] Afterwards, the remaining liquid phase of the droplet on the CG surface continues to freeze isothermally followed by slow ice growth from the droplet bottom to the top, resulting in the pointy top at the end. Strikingly, the water droplet on the ionogel surface remains in the liquid state for a longer time (97.7 s) and forms a distinctive spherical cap rather than the normal pointy cap on the other counterpart surfaces, as shown in Figure 1c. IGR in the droplet on the ionogel surface initiates from the IN sites at the droplet-air interface rather than at the droplet-ionogel interface. As shown in Figure 1c & Movie S7, a thin ice shell first forms at 100.9 s and grows thicker (130 s) toward the interior of the droplet. From 130 s to 190 s, the ice grows downward to the droplet-ionogel interface and lifts the solid droplet due to the volume expansion of water upon freezing. The red dashed curve shown in Figure 1c

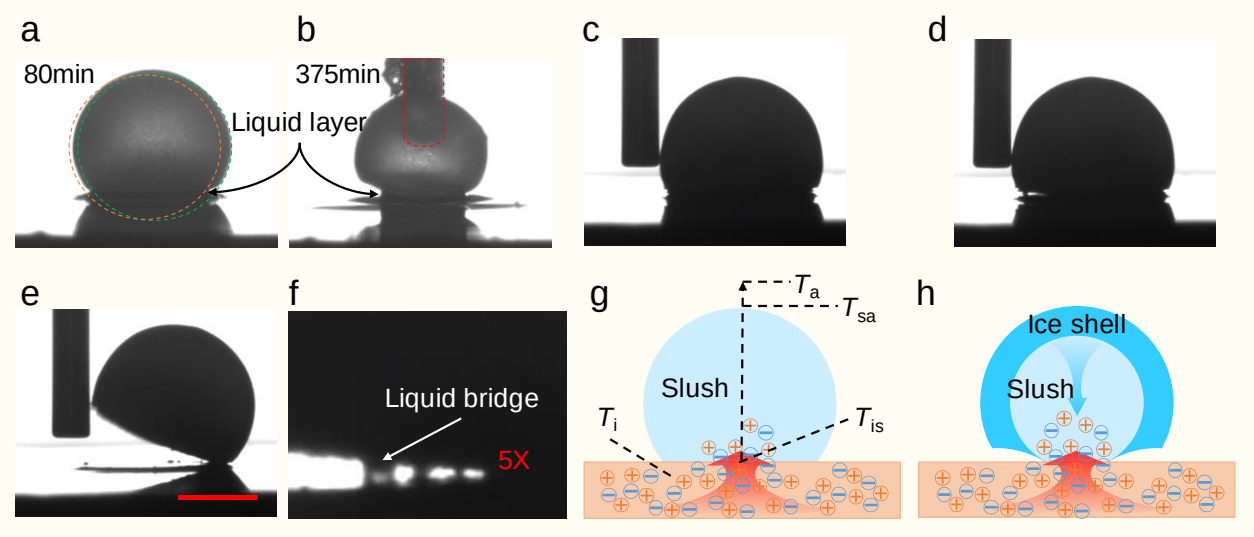

Figure 2. Dynamic melting of ice on ionogel surface at -20 °C. (a) Frozen droplet on the ionogel surface at 80 min. The green and orange dashed lines indicate the shape of the same frozen droplet at 110 and 140 min, respectively. (b) A probing needle penetrates through the ice shell and into the ice-liquid mixture core of the same frozen droplet at 375 min. (c-e) Probing needle detaching the frozen droplet from the ionogel surface. (f) Liquid bridges monitored in detaching the of frozen droplet. All the droplet images share the same scale bar of 1 mm shown in (g) (red bar). (g) Schematic showing the slush after IN and ionic liquid diffusion into the droplet on ionogel surface. (h) Schematic showing the IGR process of the droplet on the ionogel surface. The time marked in (a) and (b) is real time of the example images.

(the panel of 190 s and the inset magnified images with green frame after 190 s) is the shape outline of the droplet at 130 s, demonstrating a clear shift in the vertical direction equivalent to the lifting distance. As the IGR proceeds, the contact line of the droplet with the ionogel surface moves inwards and forms a crack at the interface due to the further lifting (370 s and 610 s, Fig 1c and Movie S8). During the course, the liquid layer at the interface thickens (Figure 2a & 2b), consequently leading to a slippery effect (the position shifting of the droplet can clearly be observed in Figure 2a & Movie S9). Such motion of the frozen droplet also indicates its ultralow adhesion to the surface, meaning that the formed ice may be removed by natural forces, such as gravity and wind shear. As shown in Figure 2a, the droplet is fully frozen at 80 min and is not penetrable by the probing needle. Surprisingly, at ~375 min, the same frozen water droplet can in fact be punctured by the probing needle (Figure 2b and Movie S10), indicating the droplet develops a liquid core internally gradually with time. The ionogel surface enables an unconventional inward ice growth from the droplet-air interface towards droplet-ionogel interface, thereby facilitating the detaching of formed ice and indicating outperforming anti-icing/anti-frost potentials.

The non-frozen liquid layer at the droplet-ionogel interface is crucial for surface icephobicity, which can effectively reduce the ice adhesion.[27, 28] To verify the presence of interfacial non-frozen liquid layer and low ice adhesion, a probing needle (outside diameter: 0.504 mm) is drawn to push the ice droplet on the ionogel surface 4 min after IN, as shown in Figure 2c-2f and Movie S11. The ice droplet is easily detached from the ionogel surface without bending the small needle, suggesting an ultralow ice adhesion strength. If the ice adhesion is high enough, the small needle can be bent significantly or broken. Additionally, liquid bridges between the ice droplet and the surface are observed in the detaching process, as shown in Figure 2f, which further confirms the presence of interfacial liquid layer and its effect of the on lowering ice adhesion.

The growth of ice from water droplet on all surfaces, including the growth direction and growth rate, depends on the release of latent heat of fusion via conduction to the substrate and/or convection to the air environment. Since conduction is much more efficient than convection, the ice favours growth upwards from the droplet-solid interface, thus forming a pointy top upon expansion for most considered surfaces like Al, glass, PMMA, CG and PDMS. The IN delay time (t_N), i.e. the interval between the time when the substrate reaches a target temperature and the time when the initial ice nuclei appears, is often taken for evaluating the icephobicity of a surface.[6, 29] Analogously, ice growth time (t_G) is taken as the time duration from the IN occurring to the droplet fully freezing, and is introduced here to quantify surface icephobicity. As shown in Figure S4, t_G on the Al, glass, PMMA, PDMS and CG surfaces shows an order of: PMMA > BIG > PDMS > CG > Glass > Al. During ice growth, the driving force is the temperature difference (ΔT) between freezing temperature (T^f) and environmental temperature (T_a). By assuming the constant interface area, the volumetric growth rate of ice ($\dot{V}$) is proportional to the heat flux ($\dot{Q}$), which is proportional to $\Delta T/R$.[30] where R is the thermal resistance between the environment and the freezing front.

$$\dot{V} \propto \dot{Q} \propto \frac{\Delta T}{R} = \frac{T^f - T_a}{R} \qquad (1)$$

Since the ΔT for all these systems are equal in this study, a decrease in R leads to an increase in $\dot{V}$. The surface with lower thermal resistance (higher thermal conductivity) provides a higher release rate of latent heat, and thus promotes faster IGR. For example, in comparison with smooth

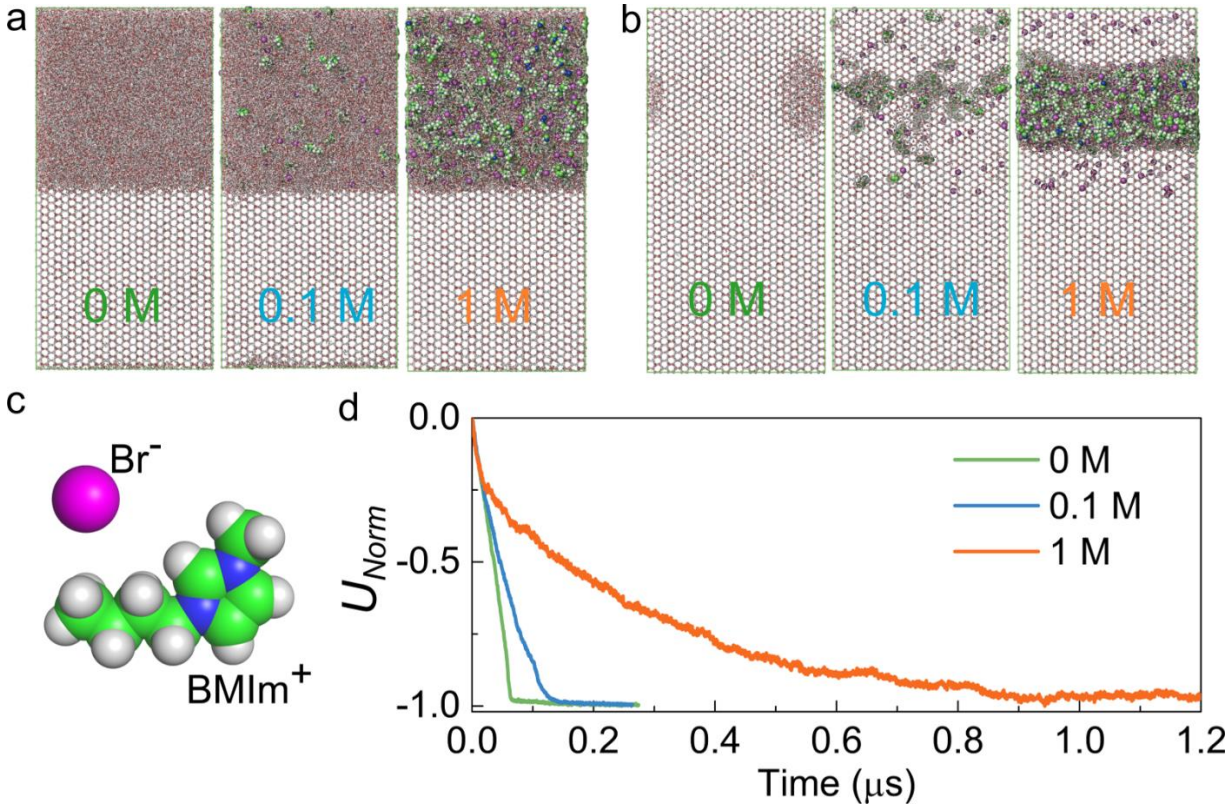

Figure 3. Ice growth with varied BMImBr concentration at 253K. (a) Initial snapshots of three systems with simulation box of half hexagonal ice and half solution containing BMImBr concentrations of 0 (pure water), 0.1 and 1 M. (b) The final snapshots of the three systems corresponding with snapshots shown in (a), with the initial BMImBr concentration labeled. (c) Atomistic structures of the Br- and BMIm+ ions, with corresponding colors in both (a) and (b). (d) Normalized system potentials (UNorm) of the three systems during the ice growth displaying the ice growth rate comparison. The potential at the initial state of each system is set to 0, and the lowest potential at the end of the simulation is set to -1. The original system potentials observed in the ice growth simulation are shown in Figure S6.

surfaces, superhydrophobic surfaces exhibit lower ice growth rate as a result of the insulating effect of the trapped air pockets.[11]

Why the droplets on ionogel surface show unique ice formation dynamics? This can be attributed to the complex interplay between ice growth and ionic liquid diffusion across the droplet-ionogel interface. As the IN occurs, the latent heat is released to the liquid phase, forming a slushy mixture of ice crystals and liquid at the temperature of 0 ºC (freezing temperature of pure water) as depicted in Figure 2g. At the time when IN occurs, the temperature at the slush-air interface, T_{sa}, and at the ionogel-slush interface, T_{is}, are approximately 0 ºC, while the temperatures of air (T_a) and ionogel (T_i) are much lower and keep the same (-20 ºC). Due to the temperature difference between slush and outside (air and ionogel), the heat can be further released to the ionogel across the ionogel-slush interface via conduction and to the air via convection simultaneously. The conductive heat transfer to the ionogel surface decreases T_{is}. However, because of the influx of ions and depressed freezing point (T_{is}^f) of the local mixed water-ion solution,[31] T_{is} is higher than T_{is}^f ($T_{is} > T_{is}^f$). Consequently, IGR can't start from the ionogel-slush interface. At the same time, the convective heat transfer to the air decreases T_{sa} and steers ice growth inwards immediately toward the core of the droplet (Figure 2h), given that T_{sa} is at the freezing temperature here (T_{sa}^f) ($T_{sa} = T_{sa}^f$). The decrease of freezing point of BMImBr aqueous solution with concentration of BMImBr is demonstrated by differential scanning calorimetry (DSC), as shown in Figure S5. The melting temperature of the aqueous solution can be lower than -50 ºC when the ion concentration reaches 1 M. Hence, with further influx of ions, the inner part of the frozen droplet can be melted. It is worth noting that the IN temperature has a maximum value as the concentration is ~0.01 M. This is attributed to the enhanced IN efficiency due to the increased fraction of ice-like water molecules. The presence of low concentration of ion can promote the structural transformation of water from liquid-like to ice-like water molecules, thus promoting the heterogeneous IN.[6, 21, 32, 33]

Atomistic modelling and MD simulations can further reveal the molecular insights of ice formation and melting and thus provide guidance for future surface design.[34-36] Herein, the all-atom model and atomistic parameters of BMImBr are taken from a former study focusing on developing OPLS Force field for imidazolium-based liquids,[37] which reproduce experimental properties of BMImBr appropriately. The tip4p/ice model is utilized for ice and water here for its precision on reproducing the water-ice phase transition.[38] As shown in Figure 3a-c, three systems with simulation boxes of half hexagonal ice and half solution with different BMImBr concentrations of 0 M (pure water), 0.1 M and 1 M are prepared and subjected to μs-scale ice growth

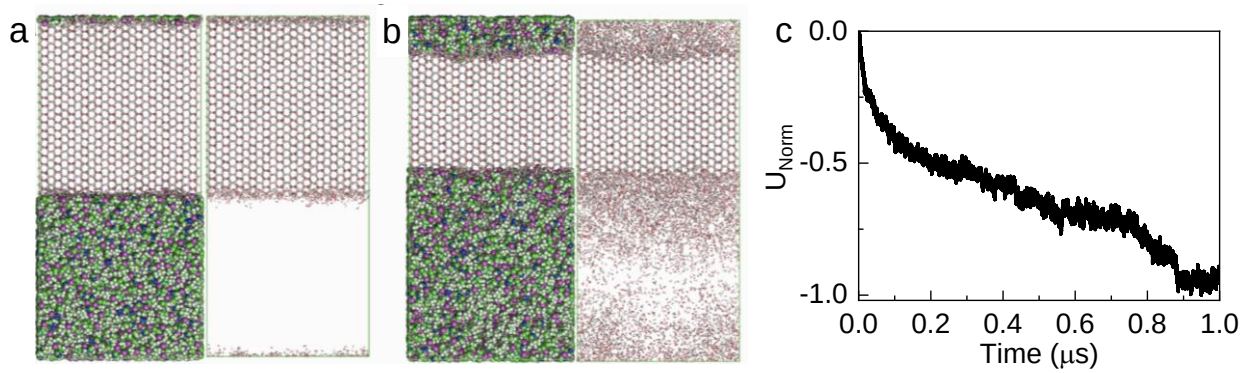

Figure 4. Melting ice by BMImBr gels. (a) Snapshots of the initial system (left), with the BMImBr molecules hidden for a clear view of the ice shown on the right. (b) Snapshots of the same system at the end of 1 μs simulation. Ice and the melted water molecules in the system are shown on the right. (c) Normalized system potential (UNorm) in the course of the ice melting.

simulations, with details given in the Experimental Section in the SI. The varied concentration of BMImBr chosen here is intended for direct comparison of its effects on delaying ice growth. All the simulations are carried out using the GROMACS (version 2018.6) package.[39]

The addition of BMImBr obviously delays ice growth at the nanoscale. The distinctive changes in the total atomistic interaction potential provide a good indication of the ice growth state and rate in the three systems, as shown in Figure 3d and Figure S6. The pure water system (0 M BMImBr) fully crystallizes in less than 70 ns, with the system potential featuring a linear decline toward a plateau corresponding to the final fully frozen state. With 0.1 M BMImBr in the solution, the system takes around 130 ns to reach a stable final state, showing a significant lower ice growth rate than pure water. The BMImBr molecules are sparsely trapped as clusters in the frozen solution (middle panel in Figure 3b). With higher BMImBr concentration of 1 M, the system strongly resists ice growth and takes roughly 1 μs to reach a stable state consisting of an ice crystal block and an amorphous mixture of ions and water (Figure 3b, right panel). As shown in Movie S12, during the freezing, the ions, especially $BMIm^+$ ions, are rejected by the advancing freezing front into the remainder of the liquid phase.[40] As a result, the concentration of ions in the remaining liquid gradually increases as the ice grows. Consequently, the system potential gradually decreases deviating from linear decline monitored in two other systems. Due to the extraordinarily high concentration of ions, a non-freezing liquid layer with highly concentrated BMImBr is formed at the final state of 1 M BMImBr system, as shown in Figure 3b (right panel), which well agrees with the experiments. It should be noted that the system potential at the final state of 1 M BMImBr solution shows clear fluctuations rather than stable values observed in two other systems, as depicted by the system potential shown in Figure 3d and Figure S6. Such fluctuations in the system potential result from the liquidity of the mixture layer with high concentration of BMImBr, as can be seen in Figure 3b (right panel). Thus, a high concentration of BMImBr is important for forming a non-freezing layer resisting complete freezing of the solution. Interestingly, the Br^- ions are easily trapped and integrated into the newly formed hexagonal ice structure (right panel in Fig 3b and Figure S7). As the larger $BMIm^+$ ions are seemingly rejected by the newly formed ice, the process of ice growth gradually separates the anions from the cations and builds up an increasing electric field against ice growth (Figure S7). Such a phenomenon observed in simulation is largely enabled by the uneven sizes and hydrophobicity of the ionic parts of BMImBr, namely Br^- is charged and water-like while $BMIm^+$ has a large hydrophobic side chain. This could be a special advantage of ionic liquids consisting of larger ions and smaller counter-ions for resisting ice growth. Generating electric field against ice growth at the ice-liquid interface is a novel molecular mechanism for anti-icing, which could be an interesting topic of future studies for new icephobic materials design and application. Especially, the result indicated the possibility of manipulating and controlling the ice growing interface in ionogel solution by external electric field.

To further demonstrate and gain physical insights of the process of ice melting and accumulation of interfacial liquid layer, simulation systems with ice and BMImBr adopting the same conditions as in the experiments (Figure 2) are constructed and investigated (details given in the SI). As shown in Figure 4a, the system initially has similar sizes as those for ice growth simulations (Figure 3), and initially contains half pure ice and half pure BMImBr gel by volume. Using the same parameters for ice growth, ice melting simulations are performed for 1 μs, with the system potential and trajectories monitored and collected. As shown in Figure 4b, at the end of the 1 μs a large portion of ice melts, and the ice structure shrinks roughly by 50%, while the BMImBr gel with melted water forms an expanding mixture (Figure 2b). Seemingly, the melted water molecules diffuse from the melting front and migrate into the BMImBr gel, which results in a decreasing water density profile away from the melting front across the whole BMImBr gel body, as shown in Figure S8. The water melting and migration in the BMImBr is energetically favorite, which can be seen by the steady decrease in the system potential given in Figure 4c and Figure S9. The BMImBr solution layer close to the ice melting front (Figure 4b) can be taken as a nanoscale replicate of the non-freezing layers in experiments. It consists of high concentration of BMImBr with water and is in an amorphous viscous state featuring liquidity. Based on the results from the ice growth and melting simulations, there should be a concentration threshold of BMImBr, which balances ice growth and melting. Both ice growth and melting with BMImBr gel possess an interfacial amorphous liquid layer

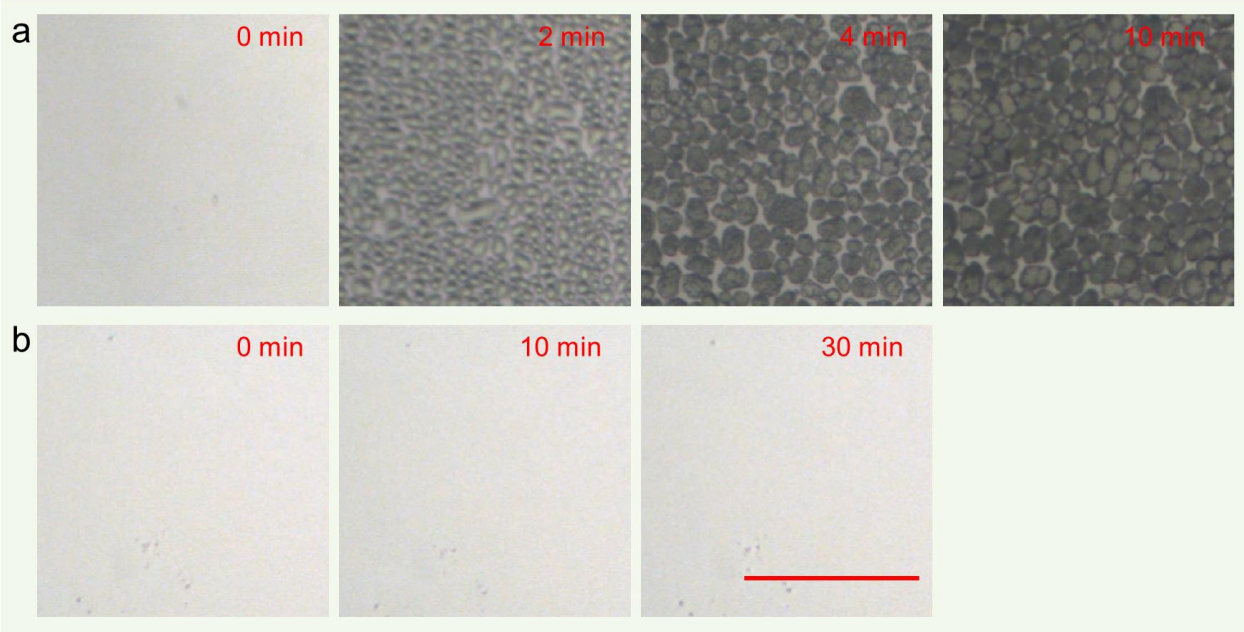

Figure 5. Comparison of condensation-frosting on glass (a) and ionogel surfaces (b). The two samples are cooled from 25 ºC to -20 ºC with a cooling rate of 10 ºC/min and then held at -20 ºC under humid environment (importing gas: 20 ºC, 60% RH). The time was recorded at the beginning of the cooling. All the figures share the same scale bar of 10 μm (red bar in (b)).

of water and BMImBr mixture, which can result in slippery interface for lowering ice adhesion.[28,41,42] Thus, BMImBr gel can restrict the formation of ice by suppress the IGR, and/or melt ice, leading to surface icephobicity.

Non-frozen interfacial liquid can grant the surface excellent icephobicity, including low ice adhesion and inhibited ice formation.[32] Due to the presence of ionic liquid and hydrophilic polymer network, the ionogel surface can absorb the water molecules from humid environments for generating a non-frozen liquid layer on the surface. Consequently, ionogel should present excellent anti-frost properties. To further verify the potential of ionogel surface for practical applications, we conduct condensation-frosting experiments, as shown in Figure S10. The samples are cooled from 25 ºC to -20 ºC with a cooling rate of 10 ºC/min and then held at -20 ºC under humid environment (importing gas: 20 ºC, 60% RH). As shown in Figure 5a & Movie S13, during the cooling process, the condensation of water vapour first occurs on the cold glass surface, followed by droplet coalescence and solidification. The glass surface is covered by small ice crystals in only 4 min and accumulates even more ice in another 10 min due to desublimation of water vapour. In contrast, there is no ice or frost forming on the ionogel surface after 30 min due to the effective inhibition in both IN and IGR, as shown in Figure 5b. Such superior anti-frost ability of the ionogel surface has not been reported to the best of our knowledge.

In summary, this work sought for an effective strategy using ionogel for inhibiting ice growth aiming to mitigate the hazards induced by excessive ice accretion. The designed ionogel surface presented outstanding abilities of suppressing ice growth and preventing frost formation in cold and humid environments. By atomistic modelling and simulations, negative and positive ions of BMImBr were observed to be separated at the ice growing front interface, which generated an electric field resisting ice growth. Either in inhibiting ice growth or in melting ice structure, the ionogel surface can form an interfacial liquid layer with at low temperature, which can lead to interfacial slippage for low ice adhesion. The design strategy and excellent properties of ionogel surface can further motivate new anti-icing and anti-frost materials. However, the mechanical robustness of this ionogel surface is not exceptional, which may hinder its widespread application. Although the ionic liquid used in this work has low environmental toxicity, its possible exhaustion after cycles of ice removal might lead to loss of icephobicity. Future works can focus on enhancing the mechanical properties of ionogel surface by incorporating energy dissipative networks, designing double-network ionogel or adding fillers and controlling the release rate of ionic liquid by molecular design.

ASSOCIATED CONTENT

Supporting Information. This material is available free of charge via the Internet at http://pubs.acs.org.
Supporting movies, experimental section, supporting figures.

AUTHOR INFORMATION

*Corresponding Author

jianying.he@ntnu.no; zhiliang.zhang@ntnu.no

† Both authors contributed equally to this work

Notes

The authors declare no competing financial interest.

ACKNOWLEDGMENT

The Research Council of Norway is acknowledged for the support to the PETROMAKS2 Project Durable Arctic Icephobic

Materials (AIM, project no. 255507), the FRINATEK project Towards Design of Super-Low Ice Adhesion Surfaces (SLICE, project no. 250990), and the Norwegian Micro- and Nano-Fabrication Facility, NorFab (project no. 245963).

ABBREVIATIONS

IN, ice nucleation; IGR, ice growth and recrystallization; MD, molecular dynamics; BMImBr, 1-butyl-3-methylimidazolium bromide; BIG, hydrophobic ionogel; Al, aluminum foil; PMMA, polymethyl methacrylate; PDMS, polydimethylsiloxane; CG, crosslinked gelatin.

REFERENCES

1. Jin, Y.; He, Z.; Guo, Q.; Wang, J., Control of Ice Propagation by Using Polyelectrolyte Multilayer Coatings. *Angew Chem Int Ed Engl* **2017,** *56* (38), 11436-11439.
2. Golovin, K.; Dhyani, A.; Thouless, M. D.; Tuteja, A., Low-interfacial toughness materials for effective large-scale deicing. *Science* **2019,** *364* (6438), 371-375.
3. Golovin, K.; Kobaku, S. P.; Lee, D. H.; DiLoreto, E. T.; Mabry, J. M.; Tuteja, A., Designing durable icephobic surfaces. *Science advances* **2016,** *2* (3), e1501496.
4. Zhuo, Y.; Xiao, S.; Håkonsen, V.; Li, T.; Wang, F.; He, J.; Zhang, Z., Ultrafast self-healing and highly transparent coating with mechanically durable icephobicity. *Applied Materials Today* **2020,** *19*, 100542.
5. Matsumoto, M.; Saito, S.; Ohmine, I., Molecular dynamics simulation of the ice nucleation and growth process leading to water freezing. *Nature* **2002,** *416* (6879), 409.
6. He, Z.; Xie, W. J.; Liu, Z.; Liu, G.; Wang, Z.; Gao, Y. Q.; Wang, J., Tuning ice nucleation with counterions on polyelectrolyte brush surfaces. *Science advances* **2016,** *2* (6), e1600345.
7. Schutzius, T. M.; Jung, S.; Maitra, T.; Eberle, P.; Antonini, C.; Stamatopoulos, C.; Poulikakos, D., Physics of icing and rational design of surfaces with extraordinary icephobicity. *Langmuir* **2015,** *31* (17), 4807-21.
8. Eberle, P.; Tiwari, M. K.; Maitra, T.; Poulikakos, D., Rational nanostructuring of surfaces for extraordinary icephobicity. *Nanoscale* **2014,** *6* (9), 4874-4881.
9. He, Z.; Zheng, L.; Liu, Z.; Jin, S.; Li, C.; Wang, J., Inhibition of Heterogeneous Ice Nucleation by Bioinspired Coatings of Polyampholytes. *ACS Appl Mater Interfaces* **2017,** *9* (35), 30092-30099.
10. Wu, S.; He, Z.; Zang, J.; Jin, S.; Wang, Z.; Wang, J.; Yao, Y.; Wang, J., Heterogeneous ice nucleation correlates with bulk-like interfacial water. *Science advances* **2019,** *5* (4), eaat9825.
11. Shen, Y.; Tao, J.; Tao, H.; Chen, S.; Pan, L.; Wang, T., Anti-icing potential of superhydrophobic Ti6Al4V surfaces: ice nucleation and growth. *Langmuir* **2015,** *31* (39), 10799-806.
12. Wilson, P. W.; Lu, W.; Xu, H.; Kim, P.; Kreder, M. J.; Alvarenga, J.; Aizenberg, J., Inhibition of ice nucleation by slippery liquid-infused porous surfaces (SLIPS). *Physical Chemistry Chemical Physics* **2013,** *15* (2), 581-585.
13. Hoose, C.; Kristjánsson, J. E.; Chen, J.-P.; Hazra, A., A Classical-Theory-Based Parameterization of Heterogeneous Ice Nucleation by Mineral Dust, Soot, and Biological Particles in a Global Climate Model. *Journal of the Atmospheric Sciences* **2010,** *67* (8), 2483-2503.
14. Montero de Hijes, P.; Espinosa, J. R.; Vega, C.; Sanz, E., Ice growth rate: Temperature dependence and effect of heat dissipation. *J Chem Phys* **2019,** *151* (4), 044509.
15. Murray, B. J.; Wilson, T. W.; Dobbie, S.; Cui, Z.; Al-Jumur, S. M. R. K.; Möhler, O.; Schnaiter, M.; Wagner, R.; Benz, S.; Niemand, M.; Saathoff, H.; Ebert, V.; Wagner, S.; Kärcher, B., Heterogeneous nucleation of ice particles on glassy aerosols under cirrus conditions. *Nature Geoscience* **2010,** *3* (4), 233-237.
16. Bai, G.; Gao, D.; Liu, Z.; Zhou, X.; Wang, J., Probing the critical nucleus size for ice formation with graphene oxide nanosheets. *Nature* **2019,** *576* (7787), 437-441.
17. Jung, S.; Tiwari, M. K.; Doan, N. V.; Poulikakos, D., Mechanism of supercooled droplet freezing on surfaces. *Nature Communications* **2012,** *3*, 615.
18. Davies, P. L., Ice-binding proteins: a remarkable diversity of structures for stopping and starting ice growth. *Trends Biochem Sci* **2014,** *39* (11), 548-55.
19. Geng, H.; Liu, X.; Shi, G.; Bai, G.; Ma, J.; Chen, J.; Wu, Z.; Song, Y.; Fang, H.; Wang, J., Graphene Oxide Restricts Growth and Recrystallization of Ice Crystals. *Angew Chem Int Ed Engl* **2017,** *56* (4), 997-1001.
20. Bai, G.; Song, Z.; Geng, H.; Gao, D.; Liu, K.; Wu, S.; Rao, W.; Guo, L.; Wang, J., Oxidized Quasi-Carbon Nitride Quantum Dots Inhibit Ice Growth. *Adv Mater* **2017,** *29* (28).
21. He, Z.; Liu, K.; Wang, J., Bioinspired Materials for Controlling Ice Nucleation, Growth, and Recrystallization. *Acc Chem Res* **2018,** *51* (5), 1082-1091.
22. Liu, J.; Zhu, C.; Liu, K.; Jiang, Y.; Song, Y.; Francisco, J. S.; Zeng, X. C.; Wang, J., Distinct ice patterns on solid surfaces with various wettabilities. *Proc Natl Acad Sci U S A* **2017,** *114* (43), 11285-11290.
23. Graeber, G.; Schutzius, T. M.; Eghlidi, H.; Poulikakos, D., Spontaneous self-dislodging of freezing water droplets and the role of wettability. *Proc Natl Acad Sci U S A* **2017,** *114* (42), 11040-11045.
24. Dash, S.; de Ruiter, J.; Varanasi, K. K., Photothermal trap utilizing solar illumination for ice mitigation. *Science advances* **2018,** *4* (8), eaat0127.
25. Katayama, S.; Fujiwara, S., NMR Study of the freezing/thawing mechanism of water in polyacrylamide gel. *The Journal of Physical Chemistry* **1980,** *84* (18), 2320-2325.
26. Chen, F.; Zhou, D.; Wang, J.; Li, T.; Zhou, X.; Gan, T.; Handschuh-Wang, S.; Zhou, X., Rational Fabrication of Anti-Freezing, Non-Drying Tough Organohydrogels by One-Pot Solvent Displacement. *Angew Chem Int Ed Engl* **2018,** *57* (22), 6568-6571.
27. Chen, D.; Gelenter, M. D.; Hong, M.; Cohen, R. E.; McKinley, G. H., Icephobic surfaces induced by interfacial non-frozen water. *ACS Appl Mater Interfaces* **2017**.
28. Chen, J.; Luo, Z.; Fan, Q.; Lv, J.; Wang, J., Anti-ice coating inspired by ice skating. *Small* **2014,** *10* (22), 4693-9.
29. Yu, Y.; Jin, B.; Jamil, M. I.; Cheng, D.; Zhang, Q.; Zhan, X.; Chen, F., Highly Stable Amphiphilic Organogel with Exceptional Anti-icing Performance. *ACS Appl Mater Interfaces* **2019,** *11* (13), 12838-12845.
30. Maxwell, J. C.; Pesic, P., *Theory of heat*. Courier Corporation: 2001.
31. Ren, Y.; Guo, J.; Liu, Z.; Sun, Z.; Wu, Y.; Liu, L.; Yan, F., Ionic liquid-based click-ionogels. *Science advances* **2019,** *5* (8), eaax0648.
32. He, Z.; Wu, C.; Hua, M.; Wu, S.; Wu, D.; Zhu, X.; Wang, J.; He, X., Bioinspired Multifunctional Anti-icing Hydrogel. *Matter* **2020,** *2* (3), 723-734.
33. Whale, T. F.; Holden, M. A.; Wilson, T. W.; O'Sullivan, D.; Murray, B. J., The enhancement and suppression of immersion mode heterogeneous ice-nucleation by solutes. *Chem Sci* **2018,** *9* (17), 4142-4151.
34. Yong, X.; Burnham, C. J.; English, N. J.; Tse, J. S., Classical and path-integral molecular-dynamics study on liquid water and ice melting using non-empirical TTM2.1-F model. *Molecular Physics* **2019,** *117* (22), 3241-3253.
35. English, N. J., Massively parallel molecular-dynamics simulation of ice crystallisation and melting: the roles of system size, ensemble, and electrostatics. *J Chem Phys* **2014,** *141* (23), 234501.
36. Burnham, C. J.; English, N. J., Communication: Librational dynamics in water, sI and sII clathrate hydrates, and ice Ih: Molecular-dynamics insights. *J Chem Phys* **2016,** *144* (5), 051101.

37. Doherty, B.; Zhong, X.; Acevedo, O., Virtual site OPLS force field for imidazolium-based ionic liquids. *The Journal of Physical Chemistry B* **2018,** *122* (11), 2962-2974.

38. Abascal, J.; Sanz, E.; García Fernández, R.; Vega, C., A potential model for the study of ices and amorphous water: TIP4P/Ice. *The Journal of chemical physics* **2005,** *122* (23), 234511.

39. Abraham, M. J.; Murtola, T.; Schulz, R.; Páll, S.; Smith, J. C.; Hess, B.; Lindahl, E., GROMACS: High performance molecular simulations through multi-level parallelism from laptops to supercomputers. *SoftwareX* **2015,** *1-2*, 19-25.

40. Vrbka, L.; Jungwirth, P., Brine rejection from freezing salt solutions: a molecular dynamics study. *Phys Rev Lett* **2005,** *95* (14), 148501.

41. Wang, F.; Xiao, S. B.; Zhuo, Y. Z.; Ding, W. W.; He, J. Y.; Zhang, Z. L., Liquid layer generators for excellent icephobicity at extremely low temperatures. *Materials Horizons* **2019,** *6* (10), 2063-2072.

42. Xiao, S.; He, J.; Zhang, Z., Nanoscale deicing by molecular dynamics simulation. *Nanoscale* **2016,** *8* (30), 14625-32.

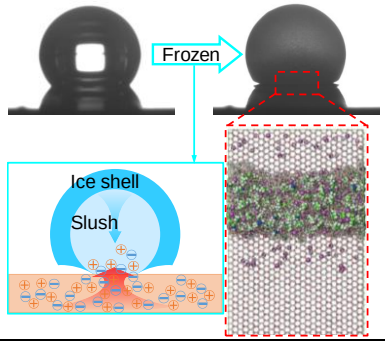
Frozen
Ice shell
Slush